Impedance spectroscopy of amorphous/crystalline silicon heterojunction solar cells under dark and illumination

Jagannath Panigrahi, Ashutosh Pandey, Shrestha Bhattacharya, Alok Pal, Sourav Mandal, Vamsi Krishna Komarala [*]

Solar Photovoltaics Laboratory, Department of Energy Science and Engineering, Indian Institute of Technology Delhi, New Delhi 110 016, India

ABSTRACT

In this article, the electronic properties of a-Si:H/c-Si heterojunction (SHJ) solar cells are analyzed by performing impedance spectroscopy (IS) characterization in the dark and under controlled illuminations. Various dynamic electrical processes occurring at different time scales, ranging from microseconds to milliseconds, are observed mainly in the operating regime of the device. Several distinct characteristics are observed: a) time constant distribution characteristic of the disordered junction, b) typical bias voltage and illumination intensity dependence of the recombination time constant, and c) an additional time constant indicative of a fast process, which appears only under illumination. The impedance spectra of the SHJ cell are best modelled by including a dispersion element, the constant phase element (CPE), in place of a pure capacitor, in its small signal electrical equivalent circuit (EEC), aside from the pure resistive and capacitive elements arranged in a simple configuration. The CPE behavior is assigned to the complex small signal response originating from the distribution of trap levels in the disordered p+-a-Si:H/n-Si heterojunction. Under illumination, a distinct dynamic process is observed compared to the dark condition in the impedance spectra of the device. The variation of the dispersion parameter, resistances, capacitance, and time constants with external stimuli is discussed. In particular, the variation of the recombination time constant with bias is remarkable under different illumination intensities due to the change in the quasi-fermi levels splitting.

1. Introduction

The solar cell performance parameters extraction usually relies on the dc current–voltage (J-V) measurements. Subsequent fitting with one- or two-diode equations gives information on series resistance (Rs), shunt resistance (Rsh), the saturation currents (J_{01} and J_{02}) and the corresponding non-ideal factors (n_1 and n_2) in the quasi-neutral and depletion regions of the cell respectively [36]. These values, however, are not enough or sometimes not very sensitive to actual electrical processes that govern the device's performance. Meaningful information may be gathered by analysing the complex dynamic impedance ($Z = Z' + iZ''$) response of a solar cell to small oscillating signals in a range of frequencies, often as a function of external stimuli [1,10,17,18,31,38], by the impedance spectroscopy (IS) technique. A solar cell's dynamic response is governed by charge accumulation, transport and recombination processes, the width of the space charge layer, and the density of trap centres. Various electrical processes happening in different cell

regions, such as diffusion and recombination in the bulk of the absorber material, interfaces, and junctions, may be simply visualized from the IS data when plotted on a complex Z'-Z'' plane, also called the Nyquist plot. One can visually distinguish the series and parallel resistances of a solar cell on the Nyquist plot, while the dc J-V curve needs diode equation fitting or comparison with the corresponding pseudo-J-V curve without the effect of series resistance obtained from a Suns-V_{oc} measurement [27]. The system then could be modelled as an electrical equivalent circuit (EEC) composed of various resistive (R_1, R_2 …) and capacitive (C_1, C_2 …) elements arranged in a simple configuration. It is essential that the EEC is based on the device's physical picture and be simple enough so that the data can be interpreted in this context. By studying the behaviour of these electrical elements with variations in external stimuli, the IS helps to understand and improve the performance of the devices, and also in the design of efficient power conditioning circuits in a photovoltaic system.

A parallel arrangement of the R and C (R||C) circuit draws a semi-

---

circular arc on the complex Z′-Z″ plot. In an IS measurement, the cell's response may appear as distinct time constants τ_i (=R_iC_i, i = 1, 2 …) corresponding to well-resolved arcs, which can be ascribed to the individual electrical processes occurring in different regions of the cell based on the physical insight. EEC constructed of simple electrical elements are helpful for systems having one or more distinct RC time constants. However, in the presence of a time-constant distribution, the above assumption is no longer valid. To explain the complex behaviour of the response from a device having disordered junctions/systems in which traps are distributed in energy and space, advanced elements such as the constant phase element (CPE) can be incorporated into the EEC model [2,6].

In contrast to the conventional diffused-junction silicon solar cells, the impedance response of the a-Si:H/c-Si heterojunction (SHJ) cell can be very sensitive to electronic exchanges with trap levels in the highly disordered a-Si:H layers. SHJ solar cells combine the high efficiency of c-Si wafer technology with the high throughput and low-temperature processing of a-Si:H thin films [7,33]. The near-perfect passivation of the silicon surface by a few nanometres thin intrinsic a-Si:H layer is the heart of such high voltage SHJ cells [5,23,35]. The stack of intrinsic and doped (p- and n-type) a-Si:H layers serve as (hole- and electron-) selective contacts. Such a-Si:H layers present band offsets and discontinuities, aside from a very high density of trap states spread throughout their band gap. Although the layers are very thin, the high density of states distributed over the entire band gap can give contributions to complex optical and electrical responses, and transport and recombination processes are likely to be different from that of the diffused-junction c-Si cell and may not be discerned using the usual J-V analysis. Hence IS is an appropriate technique for characterizing the dynamic response of the SHJ cell.

Earlier work on IS of c-Si solar cells was to resolve different capacitive and resistive elements [1,10,15,19,31] as well as to explain an anomalous negative capacitance [24] via modelling with simple EECs. Previously, IS has been adopted for the a-Si:H/c-Si HJ solar cells made on p-type silicon wafers to describe the influence of a buffer i-a-Si:H passivating layer, in which the appearance of distinct high-frequency arc was attributed to the effect of the buffer layer [8]. Aside from this, the recombination processes in SHJ solar cells under illumination have also been described in terms of distinct electron and hole capture times extracted from the IS measurements [20]. The SHJ cells in these reports had Al-alloyed back surface field as hole-selective contact; that is, only the front surface was passivated with i-a-Si:H buffer layer. Also, the influence of time constant distribution was not discussed, and the ac equivalent circuit consisted of two R||C units in a series combination. Previously, EEC with the inclusion of CPE has been used to explain the response of trap states in a-SiC/c-Si heterojunctions [25], thin film CdTe solar cells [6], and GaAs-based metal–oxidesemiconductor structures [14]. In this article, we have investigated the impedance response of both-sides passivated, complete (p/i)-a-Si:H/n-Si/(i/n)-a-Si:H front-junction SHJ solar cells having power conversion efficiency within 15–18%. We discuss the type of response from the SHJ cells that leads to the CPE behaviour. Then we pay attention to the impedance behaviour of the SHJ cell under illumination. Finally, specific focus is given to the characteristic bias and illumination intensity dependence of the recombination time constant.

2. Experimental details

The front-junction SHJ solar cells (shown in Fig. 1) in this study are fabricated from as-cut n-type Si (FZ, 2 Ω-cm, ⟨100⟩,280 μm) wafer following due procedure: pre-clean, saw damage removal (SDR), texturing, post-clean, PECVD of passivating i-layer, p-type emitter, and the n-type BSF a-Si:H layers. The cells are defined by an area of 1.7 cm × 1.7 cm ITO (~80 nm) deposited by sputtering, followed by evaporation of the Ag grid on the front. The rear side is fully covered with a stack of ITO and Al. The details of the cell fabrication and a-Si:H/c-Si interface passivation results have been reported elsewhere [22]. The impedance measurements are carried out using a Biologic SP-300 impedance
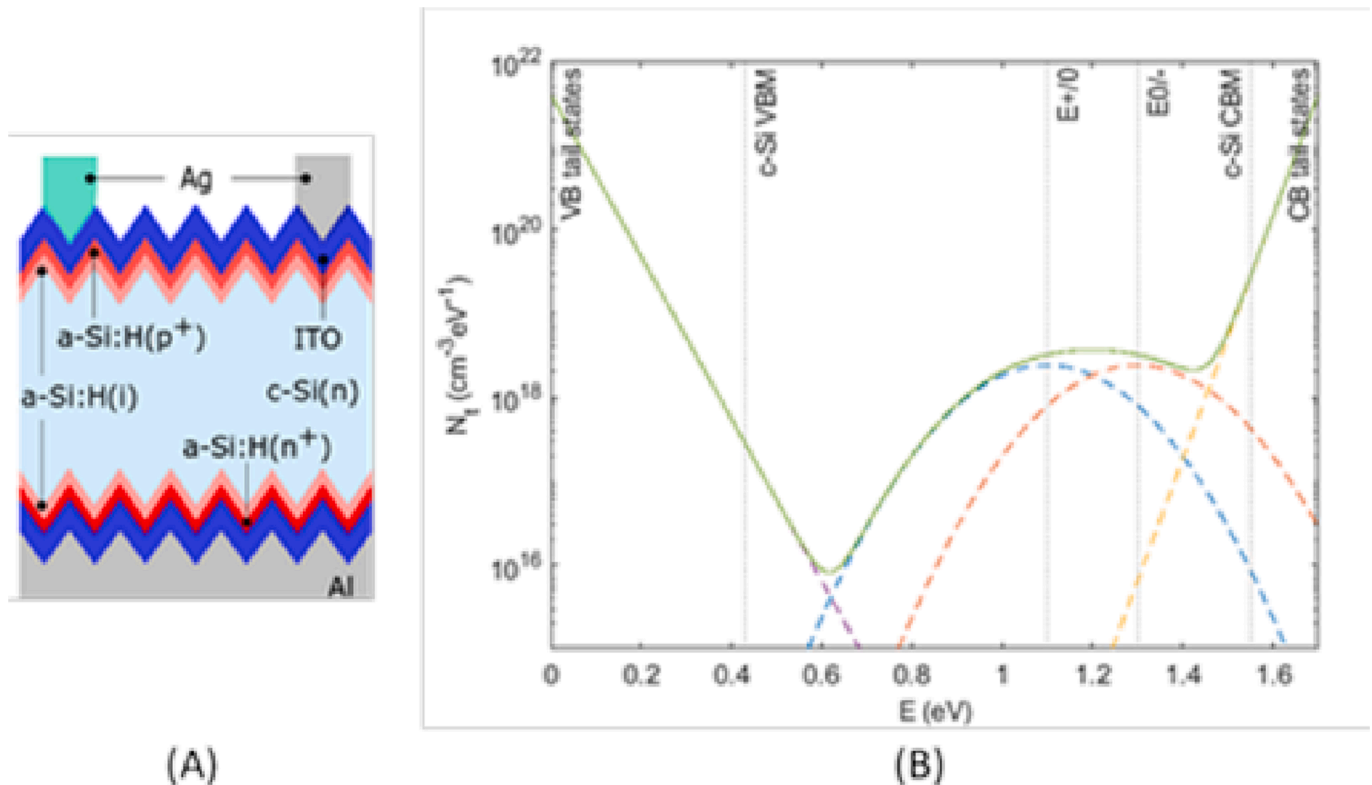

Fig. 1. (A) Schematic of the fabricated front-junction SHJ cells, and (B) a representative plot describing the characteristic distribution of the trap states in the p-a-Si:H layer according to the defect pool model [26].

analyzer in the frequency range of 1 MHz–1 Hz at different operating biases on the J-V curve in the dark as well as under different controlled illumination intensities in the range of 0.05–1.2 suns from a class AAA solar simulator (Newport Oriel, AM 1.5G). A sinusoidal oscillating amplitude of 10–20 mV is superposed over the applied dc bias offsets in the operating region of the cell. The temperature of the cell is maintained at 25 °C. The spectra are then modelled by constructing a simple EEC to interpret the data. The fitting is performed using a complex non-linear least squares regression (CNLS) technique integrated with the measurement unit. To find the best values of the parameters, that is, for a high degree of goodness of fit, the uncertainty in the chi-squared error weighted by the modulus of Z is kept within 10^{-3}–10^{-6}, and the deviation in the values of each element in the fitting is below 5%. The uncertainty in the fitting improved as the noise in the experimental data reduced.

We considered multiple SHJ cells, whose performance has been improved with wet chemical silicon surface conditioning and in the preparation of the a-Si:H/c-Si interfaces. The bulk lifetime of the c-Si is measured to be > 2 ms after passivating in a solution of iodine-ethanol by a Sinton lifetime tester. The i-a-Si:H layer passivation of the c-Si yields an effective minority carrier lifetime (τ_{eff}) above 1 ms with implied V_{OC} beyond 700 mV. The stack of p+/i-a-Si:H yields lower passivation, that is, $\tau_{eff} \sim$ 700 μs, while the stack of n+/i-a-Si:H preserves the passivation with $\tau_{eff} >$ 1 ms. The effective lifetime of the complete cells, as measured from the Suns-V_{OC} tester, ranges from 400 to 700 μs. The cells have an efficiency range of 15–18% and one-sun V_{OC} of 660–690 mV.

3. Results and discussion

A conventional diffused-junction c-Si solar cell may be considered as a standard diode. The static J-V relationship of this diode is sufficiently explained by a standard diode equation governed by the classical Shockley diffusion law, which states that the transport is limited by charge carrier diffusion in the neutral bulk. In this circumstance, the impedance spectrum of the c-Si solar cell mainly consist of a simple semicircle expressed as an equivalent circuit of the resistance R_P and capacitance C_P connected in parallel ($R_P||C_P$). In the presence of the diffusion, the diffusion capacitance is frequency dependent ($\propto \omega^{-0.5}$) [32], which would give rise to a straight oblique line (45° feature) in the high frequency portion of the Nyquist plot, it is also called the Warburg impedance [19]. This is seldom observed in the IS of real cells because of the presence of dominant parasitic inductance in the high frequencies. The R_P should agree with the differential resistance dV/dJ calculated from the dc J-V plot. However, real solar cells often require a second diode representing the generation-recombination process in the space charge region (SCR) occurring at the low-forward bias region. Similarly, Nyquist plots of real cells often require additional $R_i||C_i$ units connected with the $R_P||C_P$ element. The two-diode equation is given as [36]:

$$J(V) = J_L - J_{01}\exp\left(\frac{q(V_b - JR_S)}{n_1 kT} - 1\right) - J_{02}\exp\left(\frac{q(V_b - JR_S)}{n_2 kT} - 1\right) - (V - JR_S)/R_{Sh}$$

(1)

Where J_L is the photo-current, R_S and R_{sh} respectively are the series and shunt resistances of the cell, q is the elementary charge, and kT is the thermal energy. The saturation current densities J_{01} and J_{02} are in the quasi-neutral bulk and the SCR, respectively, n_1 and n_2 are the associated diode ideality factors.

The a-Si:H layers in the SHJ cell present a significant density of states in the band gap found as shallow-lying exponential distribution of tail states near the respective band edges, and deep-lying Gaussian-type distribution of dangling bond (DB) states in the band gap. A typical distribution of these states in the band gap of amorphous silicon is described in Fig. 1 calculated according to the defect pool model [26]. The band edges of c-Si are superimposed on the figure, considering

typical valence and conduction band offset values between a-Si:H and c-Si, 0.4 eV and 0.15 eV, respectively [12]. These discontinuities at the junction can lead to recombination, trapping, hopping conduction, and various tunnelling processes. Despite the a-Si:H layers being very thin, there are bias regimes in which the tunnelling current exceeds the bulk-limited diffusion current. Previously, using temperature-dependent J-V measurements, it has been shown that in low-forward-bias regimes, the SHJ cells are governed by carrier tunnelling and recombination processes via the distribution of states in the a-Si:H [21,30,34]. The static characteristics of an SHJ cell, though, could be modelled by the two-diode model using equation (1), however, the dynamic characteristics of a cell need complex elements to model the Nyquist plot. Also, the J-V measurement and subsequent two-diode equation cannot entirely represent the accurate physical picture of the device. So, the IS measurement is performed to investigate the transport processes which are not considered in the double-diode equation.

3.1. Impedance spectroscopy of the SHJ cells in the dark

The IS of the SHJ cells at different applied forward biases are measured and are shown in Fig. 2 as complex Z′-Z″ Nyquist plots. In
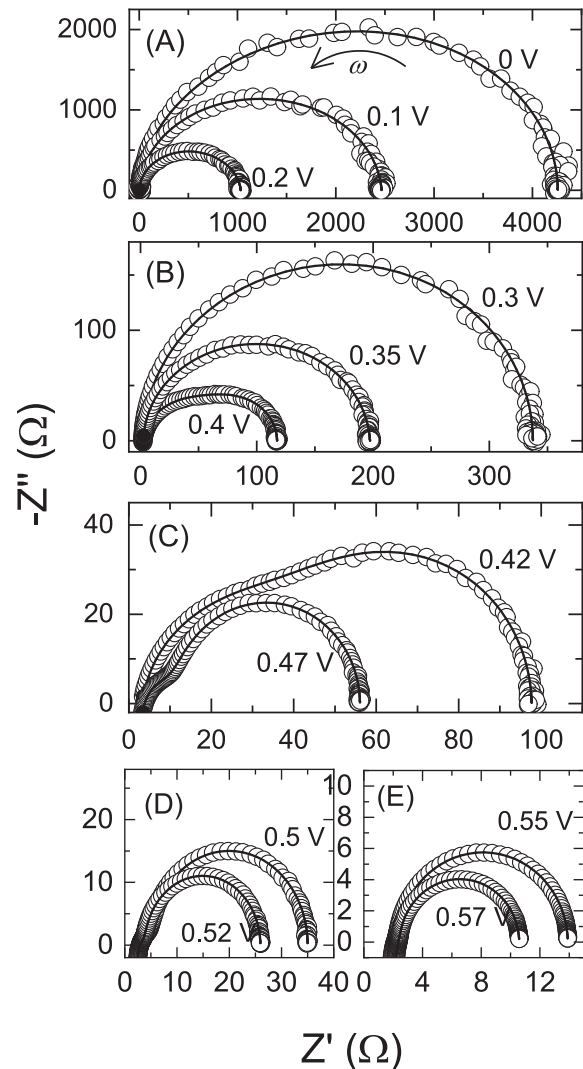

Fig. 2. Complex Z′-Z″ Nyquist plots of the SHJ solar cell measured at different bias voltages in the dark at 298 K. Symbols are the experimental data, and lines are the corresponding model fits using the dark electrical equivalent circuit of Fig. 4. The appearance and gradual predominance of the low-frequency semicircular arc are noticed after 0.4 V and above.

these plots, the Z′-axis represents the resistance component of the cell while the Z″-axis represents the reactance components related to the junction/trap/chemical capacitance and inductance. It is to be mentioned that the parasitic series resistance of the measurement set-up is measured to be $0.8 \pm 0.1 \, \Omega$ and may be subtracted from the total high-frequency series resistance RS, which appears as a displacement of the spectra from the origin on the Z′-axis. The inductive tail at the high-frequency side is represented by the series inductor LS, which is related to a parasitic inductive component such as the connecting wires and is found to be $2.6 \pm 0.1 \, \mu H$ for all the measurements. At negative and low positive voltages ($V_b < 0.35$ V), the IS spectra appear as a near-semicircular arc which shrinks in size with increasing bias as the junction becomes more conducting. For potentials more positive than 0.35 V, the arc gradually distorts into a combination of two well-resolved arcs. At higher bias ($V_{bias} > 0.55$ V), the high-frequency arc of the spectra is masked by the inductive effects, and the low-frequency arc is prevalent on the Nyquist plot. This effect could be mitigated by using smaller cells and shorter cables. As the bias increases above 0.35 V, the IS spectra begin to distort into a combination of two arcs corresponding to two different time constants representing separate electrical processes in the cell. In this bias region, the spectra could be fitted with a circuit of the series combination of R||CPE and R||C sub-circuits, shown in Fig. 4. The R||C unit is found to fit the low-frequency part of the spectra. This is clear from the -Z″ vs. frequency plots presented in Fig. 3, where the R||CPE and R||C components are superimposed as individual Z″ curves on the same plots. The characteristic frequency ω_t of the R||CPE sub-circuit shifts towards a higher frequency as the bias voltage increases, whereas that of the R||C sub-circuit shifts to lower frequencies. From the change of ω_t with V_b, it may be assumed that the CPE response comes from a distribution of the shallow lying exponential tail-like states near the heterojunction according to the relation [2,39]:

$$\omega_t(E_t) = v_{th}\sigma_n N_t exp[-(E_f - E_t)/k_B T] \tag{2}$$

Where E_t and N_t are respectively the energy and density of the trap level, v_{th} and σ_n are the electron thermal velocity and capture cross-section, and $k_B T$ is the thermal energy. As the bias voltage is varied, the occupancy of trap levels changes, which appears as the voltage dependence of ω_t in Eq. (2). The appearance of the low-frequency arc, which comes into the equation at sufficient positive voltages, has earlier been assigned to the impedance response of the rear low–high junction in the case of the c-Si homojunction solar cell [4,10], or due to the chemical capacitance of the minority carriers [19,20]. The low-frequency arc is an indicator of the accumulation of minority carriers in the absorber, which leads to a chemical capacitance and, therefore, is related to the carrier recombination processes.

The EEC is constructed considering the disordered nature of the junction, and the devices IS spectra, as shown in Fig. 4. In the EEC, the R_{tr}||CPE subcircuit models the transport dynamics of the disordered heterojunction. The resistive component is the transport resistance R_{tr} mainly the impedance of the junction, representing the energy barrier presented to the electrons from the n-Si side or to the holes from the p-a-Si:H side. R_{tr} encompasses the behaviour of the exponential-tail-like distribution of shallow trap states in the a-Si:H layers assisting in charge transport, for instance, the release of an electron to the extended levels above the conduction band E_c. C_{tr} is the pseudo-capacitance equivalent of the CPE and represents junction capacitance arising from the changes in occupation level of the exponential distribution of trap levels in the disordered a-Si:H layers. In the R||C subcircuit, which represents the recombination dynamics of the charge carriers, R_{rec} represents the recombination resistance and C_μ represents the chemical capacitance due to the accumulation of the minority carriers in the forward bias. In literature, it was assigned the chemical capacitance of electrons and holes [20] or capacitance of the p-n junction and low–high junction, respectively [10]. Rather than naming the corresponding time constants to the capture time of electrons and holes, here we denote the time constant corresponding to the R||CPE subcircuit as the transit time
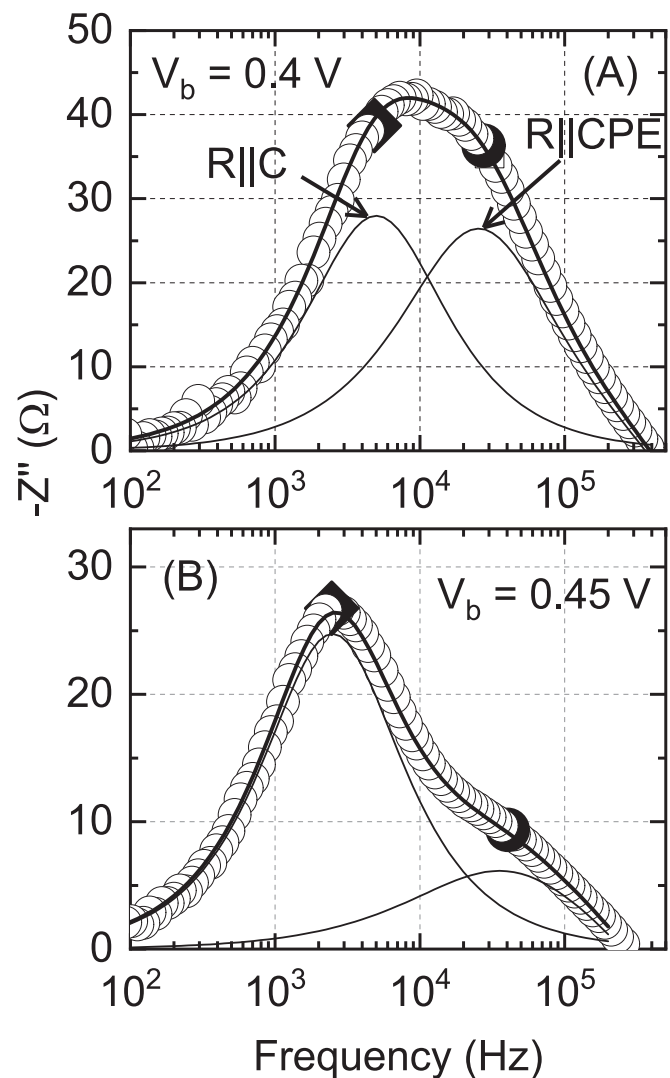

Fig. 3. Frequency dependence of the imaginary component Z″ compared for two different bias voltages showing superposition of the individual Z″-f curves from R||CPE and R||C sub-circuits (lines). Symbols are the experimental data, and lines are the EEC fitting. The corresponding characteristic frequencies are shown as filled symbols.

or time of transport (τ_{tr}), i.e., the time taken by a charge carrier to transit across the cell. The time constant of the R||C sub-circuit is named recombination time (τ_{rec}).

The CPE is included in the EEC in place of a pure capacitor to model the depressed high-frequency arc in the IS (Fig. 3). The circuit is meant to represent a regular double diode, whose conduction at high frequencies is modified by the carrier trapping and relaxing process represented by the CPE. The origin of the CPE behaviour, which is still a subject under discussion, is generally ascribed to various material in-homogeneity [40]. CPE has often been used in electrochemical systems to describe relaxation processes with reactivity distribution and surface heterogeneity of solid electrodes [11]. The time constant distribution might arise due to variation of some physical properties, either parallel or normal to the surface of an electrode. Recently, the origin of the CPE behaviour in the impedance studies of solid electrodes has been critically reviewed [16], and it was attributed to the adsorption of a trace amount of impurities at the micro-rough electrode surfaces. In disordered solids such as amorphous semiconductors, the distribution arises because of localized states' energetic and spatial distribution [2]. Each localized state in the band gap introduces one R-C time constant, so the time constant distribution results in a significant capacitance dispersion.
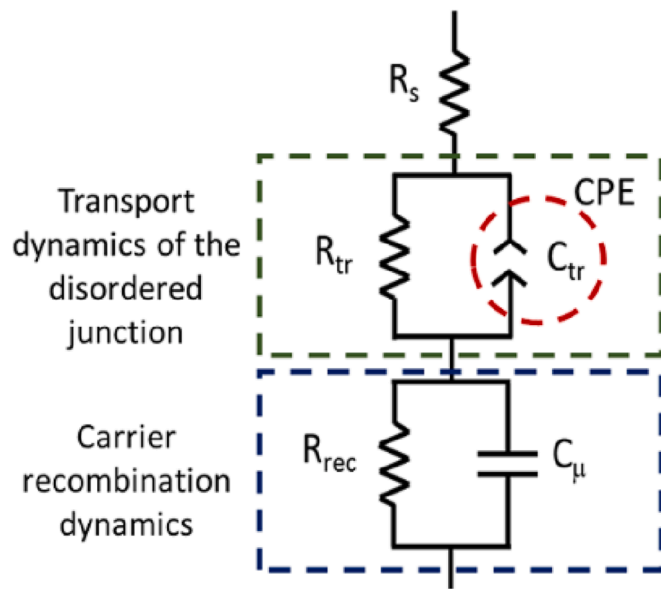
Fig. 4. The small signal electrical equivalent circuit (EEC) of the SHJ cell for fitting the impedance spectra. At low bias, the R||CPE unit sufficiently models the impedance response, while at moderate and higher forward bias, the entire unit is required to fit the spectra. The R||C unit is required at a higher forward bias. R_S is the total series resistance, including those of the connecting wires. The series inductor Ls is not included in this schematic; however, it is always required to model the IS spectra completely.

Overall, the CPE seems to result from a two- or three-dimensional time constants distribution. The distribution in the relaxation time yields a depressed semicircle on the Nyquist plot. The CPE can be considered as a frequency-dependent non-ideal capacitor. The CPE has the impedance: $Z_{CPE} = 1/[Q(i\omega)^{\alpha}]$ for $0 < \alpha < 1$, where α is a dimensionless dispersion parameter with a value between zero and unity, and $i=\sqrt{(-1)}$. Q is the frequency-independent non-ideal parameter. For $\alpha = 1$, the impedance effectively reduces to the value of a pure capacitor, while for $\alpha = 0$, it is that of a real resistor, and if $\alpha = 0.5$, the CPE reduces to the Warburg element whose impedance tends toward a straight oblique line. In the impedance response of the SHJ cell, the CPE represents the disordered nature of the a-Si:H layers and a-Si:H/c-Si interface in which traps are distributed in energy and space.

The resistive components R_{tr} and R_{rec} from the IS analysis, and

differential resistance dV/dI calculated from the J-V curves based on the dc applied voltage are shown in Fig. 5. The dark and illuminated J-V curves are shown for a representative cell. Apart from the series resistance, while the dc J-V curve gives only one differential resistance of the device, IS distinguishes between different parallel resistances from various sources in the same device. It is seen that although the dV/dI tends to saturate at a low value towards higher bias, the parallel resistance components of the cell can still be obtained from the impedance spectrum. The resistances vary with bias voltage according to the following relation [10,31]

$$\ln(R_{tr}) = \ln(R_0) - \left(\frac{eV_b}{mkT}\right) \qquad (3)$$

Where R_0 is a voltage-independent constant. It could be seen that in the low bias region, the impedance is primarily the R_{tr} while R_{rec} starts to appear and then dominate the R_{tr} after a moderate voltage of 0.35 V. The close agreement between R_{tr} and dV/dJ in the bias region of interest assures that the impedance measurement is in line with the dc J-V measurement and does not include any noticeable artefacts or absence of any other unexplainable phenomena.

The values of capacitive elements are extracted and are shown in Fig. 6 as a function of bias voltage. C_j is the pseudo-capacitance equivalent of the CPE ($=\omega_p^{\alpha-1} /Z_{CPE}$, where ω_p is the peak frequency in the Z″ spectra). From the figure, it is noticed that C_j (or Q) behaves similarly as a junction capacitance, having the components like the depletion capacitance feature at lower bias, and the diffusion capacitance at higher bias, readily observed as a change in the slope of C_j, exhibiting an exponential dependence according to the relation [10,31]

$$\ln(C_j) = \ln(C_0) + \left(\frac{eV_b}{nkT}\right) \qquad (4)$$

Where C_0 is voltage independent, and 'n' is an ideality factor of the cell. The region of higher bias is usually denoted as the chemical capacitance [19]. There is a noticeable hump near 0.35 V, at which the distortion in the impedance arc is observed. The inset shows the frequency-independent constant Q of the element CPE with similar behaviour as that of the capacitance C_j. A discussion of its physical significance is beyond the scope of this article. The other capacitance C_μ is the chemical capacitance associated with the recombination process, arising at moderate to higher forward biases and could be called the chemical capacitance of holes. The homogeneous accumulation of minority carriers in the bulk of the wafer leads to the splitting of the Fermi
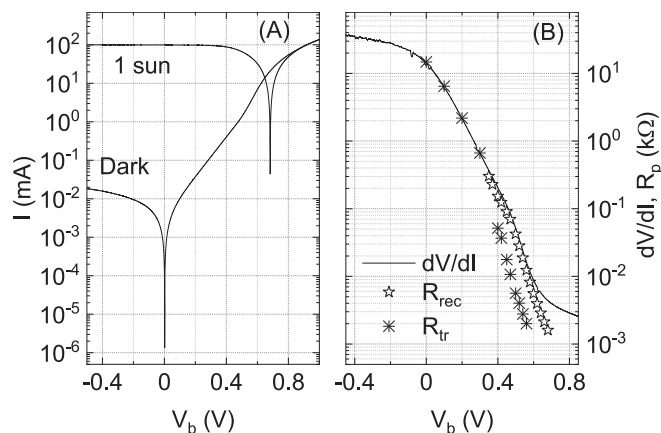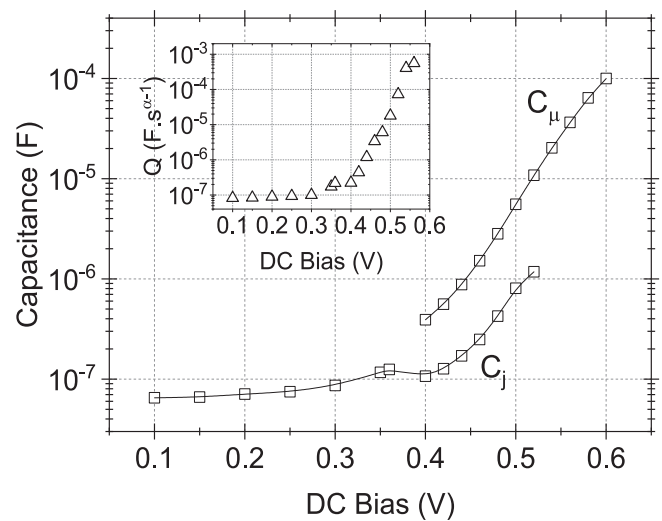

Fig. 5. (A) Semilogarithmic plot of the J-V characteristics measured in the dark and under 1 sun illumination intensities of an SHJ cell. (B) The differential resistance $(dI/dV)^{-1}$ (continuous lines) was calculated from the dark J-V plot, and the parallel resistances (symbols) were obtained from the fitting the IS measurement data at different voltages.

Fig. 6. The capacitive elements C_j and C_μ as a function of bias. The inset shows the CPE's frequency-independent non-ideal parameter Q as a voltage bias function.

levels, and C_μ is related to this splitting as,

$$C_\mu = q^2 W p_0 \exp\left[\frac{q(E_{Fn} - E_{Fp})}{nkT}\right] \Big/ kT \qquad (5)$$

Where 'W' is the thickness of the c-Si wafer, p_0 is the equilibrium hole concentration, E_{Fn} and E_{Fp} are the quasi-Fermi levels of electrons and holes, respectively, and kT is the thermal energy. The slope of the linear fit in the C_μ vs V_b plot could be an indicator of the cell's ideality factor 'n'. Therefore, a change in the slope relates to the quality of the interface/junction formed. Aside from the high bulk lifetime silicon, high-quality passivation of the silicon surfaces by the i-a-Si:H layers leads to very high C_μ values.

3.2. Impedance spectroscopy under controlled illumination

Fig. 7 shows representative impedance spectra in terms of both the Nyquist plot and the frequency dependence of Z″ to distinguish the small signal response of the SHJ device under illumination. The size of the arc decreases with increasing illumination levels. It is seen that under illumination, the spectra are stretched along the Z′-axis compared to the spectra under dark. For a typical spectrum under dark, for $V_b = 0.42$ V in Fig. 2 for example, the condition at which the spectra are distorted the most, Z′ is less than three times Z″. While under illumination Z′ is more than three times Z″. Therefore, the spectra under illumination have possibly more than two-time constants, and a satisfactory CNLS fit is actually obtained by including another R′||C′ unit in series to the EEC considered under dark, explained in Fig. 4. The EEC of the SHJ cell under illumination is shown in Fig. 7c. The broadening is also noticed in the Z″-f plot (Fig. 7b). The characteristic frequency of this R′||C′ is higher than that of the R||CPE, as is apparent from the frequency dependence of Z″. When the MPP condition is reached for the cell at each illumination, the impedance of the R′||C′ circuit is overwhelmed by the impedance response of the other units as well as the parasitic inductor component and, therefore, can no longer be distinguished. The time constant τ′ (=R′C′) corresponding to the R′||C′ unit, which is observed only under illumination, is also a transport time and is of the order of only a few microseconds. Therefore, it is indicative of a faster transport process. At

present, it is not clear which type of tunnelling or transport channel this unit represents, as many transport phenomena are expected to compete; see, for example, [21,30,34]. Considering another possibility, it can also be the response due to the transport at the p-a-Si:H/ITO interface. Because usually, the ITO has a lower work function ($\Phi \sim 4.7$ eV) [13] than p-a-Si:H ($\Phi \sim 5.1$ eV) [37], a Schottky barrier or a hole depletion layer is formed at the p-a-Si:H/TCO interface which hinders the hole transport [3,29]. However, the ITO/p-a-Si:H interface is generally assumed to be a part of the total R_S of the SHJ cell.

As the characteristic frequency response of the R||CPE sub-circuit is in the order of 10 kHz, it is a characteristic of a fast transport process, and we assume that the CPE response results mainly from the existence of the exponential distribution of shallow trap states near the band edges resulting in distributed time constants. The dispersion parameter α, is assumed to denote the extent of distribution of the trap states in the band gap. The variation of the dispersion parameter α with V_{bias} is shown in Fig. 8. As shown in the figure, its values are close to 1, that is, in the range of 0.97–0.95 at the reverse and low forward bias. This means that the heterojunction behaves close to a capacitor but does not reach the ideal case because of the presence of disorder in the amorphous silicon. It drops from 0.95 to 0.65 as the bias is increased above 0.35 V. It is lowest (α ∼ 0.6) at voltages around 0.5 V. The values above 0.55 V bias are not considered because the masked impedance of the R||CPE unit is prone to high fitting errors. Under illumination, however, note that the variation in α is significant, reaching values close to 0.6 at even intermediate bias levels, demonstrating that the trap states actively participate in the transport process. Also, a pronounced effect, that is, the lowest values of α is found at the intermediate illumination level (at 0.5 suns). It is difficult to explain the nature of processes responsible for the existence of CPE with such a low value of α at this moment; nevertheless, excellent fits to the experimental data are obtained in a broad range of frequency, bias voltage, and illumination. It may be suggested that, aside from carrier generation and recombination, illumination also activates some deep traps, and this process is enhanced under some intermediate illumination intensities. In the dynamic electrolyte–electrode systems, which are governed by a characteristic diffusion process, CPE with α values close to 0.5 are frequently encountered. Therefore, the existence of low values of α at higher bias voltages and under illumination suggests a contribution to the trap-assisted diffusion phenomenon or the activation of some traps. In this case, it may be suggested that the response from a broad distribution of states gives rise to a lower value of α.
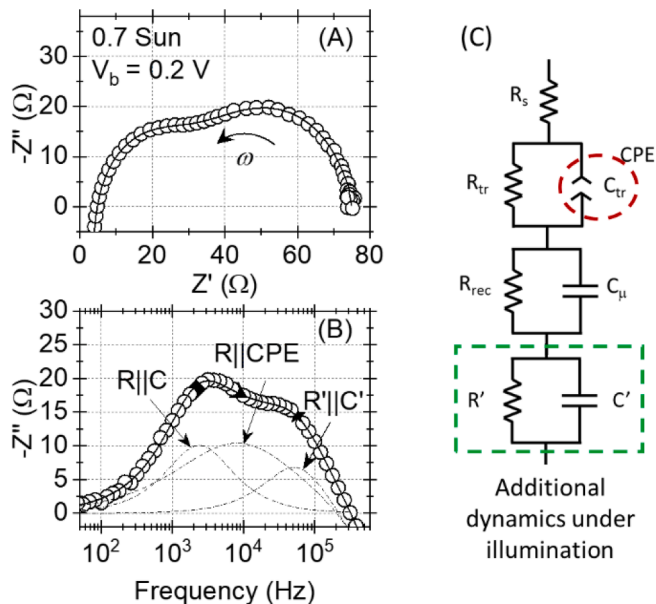

Fig. 7. (A) Representative impedance spectrum, and (B) frequency dependence of the imaginary part Z″ of the SHJ solar cell recorded at a bias of 0.2 V under the illumination of 0.7 sun. Symbols are the experimental data, and lines are the corresponding EEC model fits. (C) The EEC of the SHJ cell under illumination describes the appearance additional R′C′ unit.
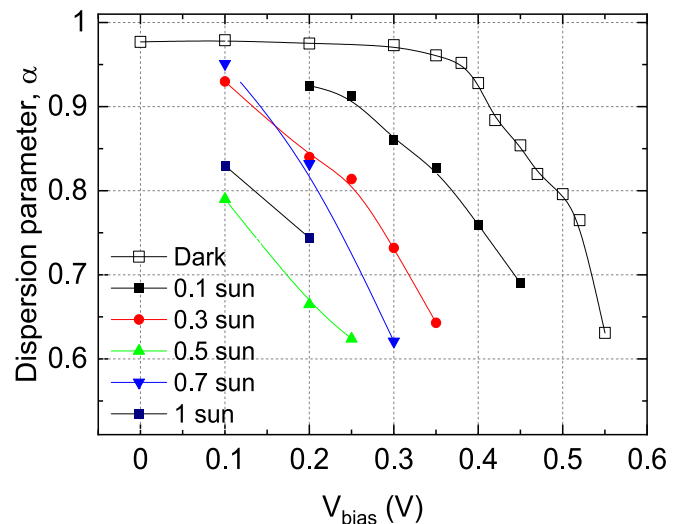

Fig. 8. Plot of the dispersion parameter α as a function of dc bias voltage extracted from the fitting of the IS data recorded in the dark and under different illumination intensities.

Lower values of α, either at higher forward bias or under illumination, also correlate to very high dispersion in the capacitance spectra of the cell. Considering the type of distribution that affects the dispersion of capacitance, it is seen that at a more positive bias, the dispersion in the capacitance changes from a broad and continuous type to a pronounced step. The capacitance dispersion is very high under illumination. This is apparent from the dispersion parameter α, which starts to decrease. It has been shown that a Gaussian distribution of traps results in a pronounced step in the capacitance spectra, whereas a tail-like distribution gives rise to a less steep and broad dispersion [39]. In this case of the SHJ cell, the dispersion can be supposed to be a superposition of Gaussian as well as tail-like distribution of traps.

3.3. Time constants of the cell under dark and illumination

The typical variation of the time constants τ_{tr} and τ_{rec} for different SHJ cells are extracted from the dark IS data, which are shown in Fig. 9B as a function of bias along with the one-sun J-V graphs of the cells (Fig. 9A). The performance of the SHJ cells has been improved by optimizing the wet chemistry in silicon surface preparation and the PECVD of i-a-Si:H layers. The difference in the performance of the

Fig. 9. (A) Illuminated J-V curves of the three SHJ cells, (B) Dark time constants τ_{tr} and τ_{rec} extracted from the IS of the same SHJ cells plotted as functions of bias voltage.

multiple SHJ cells could be noticed from the bias dependence of the time constants in the dark, particularly the variation of τ_{tr} in the low forward bias region. It is observed that in the dark, τ_{tr} decreases with an applied dc voltage, similar to the parallel resistance R_{tr}. The $\tau_{tr}(V)$ curve can be assumed to follow the relation:

$$\tau_{tr}(V) \propto exp(-qV_b/mk_BT) \tag{6}$$

For instance, τ_{tr} has values of about 200 μs, 400 μs and 900 μs at zero bias for SHJ-35, SHJ–41 and SHJ–116 cells, respectively. From the respective values at low forward bias, τ_{tr} reduces to a few microseconds near 0.5 V. This time constant is mainly determined by the R_{tr} rather than the pseudo-capacitance C_{tr}. It is identified from measurement on multiple cells that the slope or the factor 'm' depends on the quality of the interface/junction formed; that is, the higher the R_{tr} of the cell at low bias voltages, the better the cell performance. The low forward bias τ_{tr} is dominated by recombination in the SCR region, possible recombination centres being at the a-Si:H/c-Si interface and in the bulk of a-Si:H layer. With improvement in the interface and junction quality, the density of these recombination centres is reduced, which is reflected in the enhanced values of τ_{tr} of the three cells.

The low-frequency arc has a pure RC time constant τ_{rec}. In contrast to τ_{tr}, the τ_{rec} (V) exhibits opposite behaviour, which nearly exponentially raises with the bias voltage up to a certain value, a behaviour very similar to the voltage dependence of the chemical capacitance C_μ. Therefore, τ_{rec} is primarily governed by the C_μ. Under dark, the dependence of τ_{rec} on the applied bias is assumed to be governed by the proportionality equation:

$$\tau_{rec,dark}(V) \propto exp(qV_b/mk_BT) \tag{7}$$

τ_{rec} raises from a low value of 30–40 μs at moderate forward bias and saturates at a higher bias near the values of 400–700 μs, and a higher value is obtained for a cell having better surface passivation as well as high V_{OC}. This saturation lifetime value is similar to the effective lifetimes of the respective cells measured by the QSSPC technique under open-circuit conditions. The bias voltage at which the τ_{rec} saturates is also increased with increasing V_{OC} of the SHJ cell. Earlier, a U-shaped time constant variation with bias voltage has been determined for diffused-junction silicon solar cells with Al-alloyed BSF [4], and it was explained in terms of varied contribution of charge-carrier recombination in the space charge region, bulk, and the back surface with bias voltage.

Notably, we also have observed a typical illumination intensity dependence of the recombination time constant. The behaviour of τ_{rec} for the SHJ cells at different bias voltages under different illumination intensities is shown in Fig. 10. It is seen that the variation of τ_{rec} with bias voltage has an illumination intensity dependence. When light is weak, the result is dominated by dark recombination. As the illumination level increases, the dark recombination is gradually suppressed, as a result of generation and accumulation of charge carriers in the bulk. At one sun illumination, the bias dependence of the τ_{rec} is more or less suppressed, and the curve nearly flattens. It may be suggested that under illumination, τ_{rec} varies with bias V_b as:

$$\tau_{rec,light}(V_b) \propto exp(qV_b/m'k_BT) \tag{8}$$

Where m' is some function of the illumination intensity. In the dark, m' approaches the value of m. The experimental data in Fig. 10 could be fitted with a fourth-order polynomial, the physical significance of which needs further analysis. The lifetime values increase at each illumination as the open-circuit voltage (V_{OC}) and fill factor are improved as a result of the optimization of cell processing. It is found that the τ_{rec} determined either in the high forward bias or under different illumination intensities at open-circuit (OC) conditions compared closely with the effective carrier lifetime of the complete cell as measured by the Suns-V_{OC} technique. $\tau_{eff} \approx \tau_{rec} \approx 700$ μs for SHJ-116, for example. The lifetime measurement gives an indication of the recombination at the open-circuit
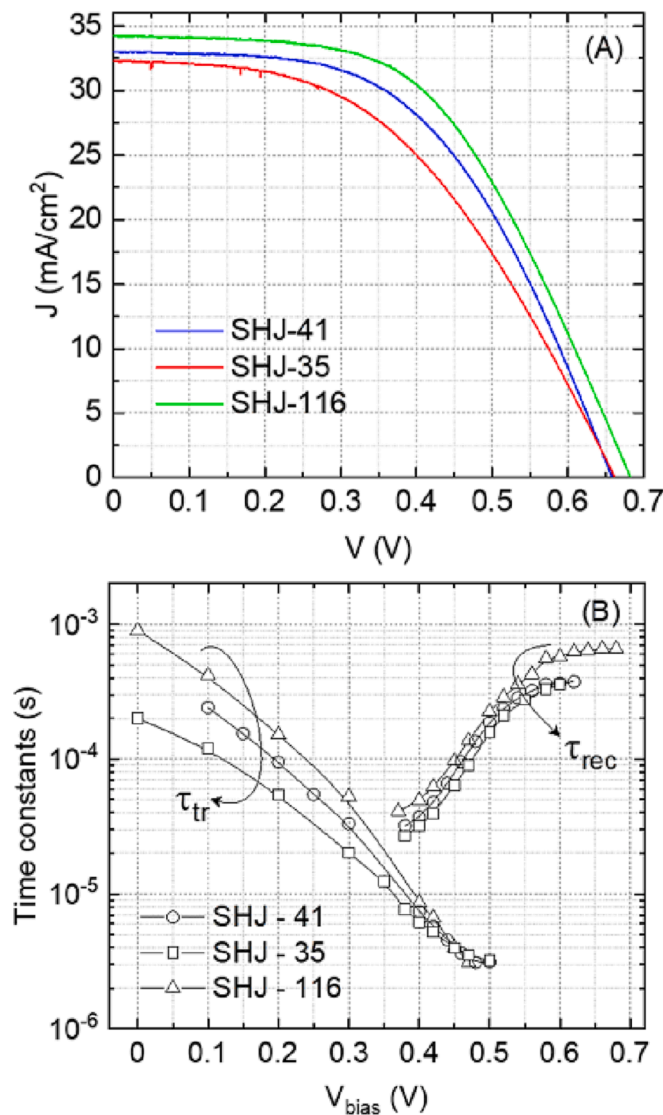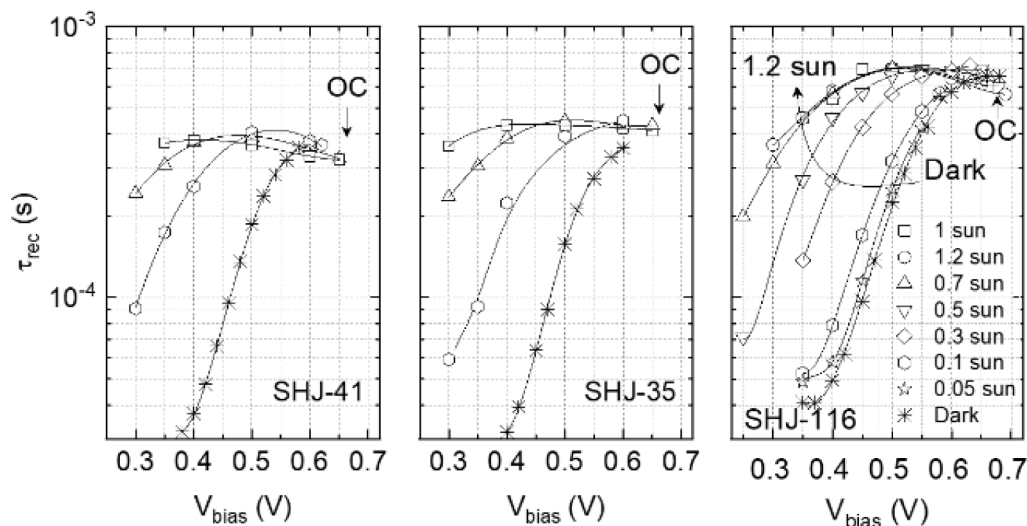
Fig. 10. Variation of the recombination time constant τ_{rec} of the SHJ cells with bias at different illumination intensities. The lines are the fourth-order polynomial fits to the experimental data. Cell open-circuit (OC) conditions are marked on each plot.

conditions in a range of illumination intensity.

The dark J-V curves of the three SHJ cells have been fitted with the two-diode model using the 2/3-Diode Fit program from nanoHub resources [28] and the extracted parameters are listed in Table 1. It is evident that with an improvement in surface conditioning and i-layer passivation, the J_{01} and the associated ideality factor n_1 of the cells improve, which is also seen as an increment in the cell V_{oc} and recombination time constant τ_{rec}. Despite having similar V_{oc}, the higher J_{01} of SHJ-35 than SHJ-41 is because of its processes. The large values of J_{02} and n_2 at moderate forward bias conditions related to the second diode represent the SCR; under this bias condition can make $J_{02} \gg J_{01}$ along with a significant ideality factor. Regarding the diode ideality factors, a careful examination of the ideality factors in Eqs (3)-(8) reveals that only the factor in eq. (4) or eq. (5) has values close to that of n_1 in eq. (1). The values of n are listed in the table. All other ideality factors mentioned in Eqs (3)-(8) have values within 1.5 to 3.5 and are not associated with the actual diode ideality factors of eq. (1). These values can be categorized into an effective factor 'm', arising out of a coupled-defect recombination mechanism, as described in the work of Garland et al. [9] and the references therein. The factor m' of eq. (8) is, however, some function of illumination intensity, and requires further evaluation for a detailed understanding, which is beyond the scope of this work. The IS measurement explains the behaviour of the solar cell under real operating conditions, that is, under varying illumination and at different biases. It is to be noted that the general dynamic behaviour of the SHJ solar cell is confirmed for multiple cells. In particular, the appearance of a CPE in the EEC of the SHJ cell, the dispersion parameter, and the typical variation of the time constants with voltage have not been previously mentioned in the earlier reports of IS characteristics of the SHJ cell.

4. Conclusions

The impedance response of the disordered a-Si:H/c-Si heterojunction has a time-constant distribution, which could be successfully modelled by incorporating a CPE in place of a pure C in the EEC. In comparison with the IS of a standard homojunction c-Si solar cell, in which a CPE is seldom incorporated in its EEC, the necessary requirement of a dispersion parameter to model the IS of the SHJ cell indicates a broad distribution of time constants, that is, a shallow distribution of exponential tail-like trap centres in the amorphous layer or/and c-Si/a-Si:H interface, especially at the front junction. Although the physical meaning of the dispersion parameter α is yet to be explained, we believe that further analysis is essential for a better understanding of the electronic processes

Table 1
Saturation current densities and ideality factors.

Device	V_{oc} (mV)	$J_{01}(\times 10^{-12}$ A/ cm^2)	$J_{02}(\times 10^{-6}$ A/ cm^2)	n_1	n_2	n from C_μ-V plot
SHJ-35	662	98.0	1.09	1.33	3.24	1.36
SHJ-41	660	14.6	1.97	1.19	3.55	1.25
SHJ-116	685	2.70	1.32	1.13	3.29	1.18

at the heterojunction. Under illumination, the spectra are observed to contain an additional high-frequency RC time constant, which remains active in the low-bias region, and is attributed to a tunnelling transport channel. The variation of the recombination time constant with bias voltage has a typical illumination intensity dependence. Thus, impedance spectroscopy is a useful tool in analyzing various electrical processes in an SHJ cell. By monitoring these electrical parameters with temperature and illumination, and comparison with heterojunction modelling, the mechanism governing the cell performance can be explained further for augmenting the power conversion efficiency of the heterojunction cells during process optimization.

Declaration of Competing Interest

The authors declare that they have no known competing financial interests or personal relationships that could have appeared to influence the work reported in this paper.

References

[1] Anil Kumar, R., Suresh, M.S., Nagaraju, J., 2000. Measurement and comparison of AC parameters of silicon (BSR and BSFR) and gallium arsenide (GaAs/Ge) solar cells used in space applications. Sol. Energy Mater. Sol. Cells 60, 155–166. https://doi.org/10.1016/S0927-0248(99)00080-X.

[2] Bisquert, J., 2008. Beyond the quasistatic approximation: Impedance and capacitance of an exponential distribution of traps. Phys. Rev. B 77, 235203. https://doi.org/10.1103/PhysRevB.77.235203.

[3] Centurioni, E., Iencinella, D., 2003. Role of front contact work function on amorphous silicon/crystalline silicon heterojunction solar cell performance. IEEE Electron Device Lett. 24, 177–179. https://doi.org/10.1109/LED.2003.811405.

[4] Crain, D.J., Garland, J.E., Rock, S.E., Roy, D., 2012. Quantitative characterization of silicon solar cells in the electro-analytical approach: Combined measurements of temperature and voltage dependent electrical parameters. Anal. Methods 4, 106–117. https://doi.org/10.1039/c1ay05455d.

[5] De Wolf, S., Descoeudres, A., Holman, Z.C., Ballif, C., 2012. High-efficiency Silicon Heterojunction Solar Cells: A Review. Green 2, 7–24. https://doi.org/10.1515/green-2011-0018.

[6] Friesen, G., Özsar, M., Dunlop, E., 2000. Impedance model for CdTe solar cells exhibiting constant phase element behaviour. Thin Solid Films 361–362, 303–308. https://doi.org/10.1016/S0040-6090(99)00764-6.

[7] Froitzheim, A., Brendel, K., Elstner, L., Fuhs, W., Kliefoth, K., Schmidt, M., 2002. Interface recombination in heterojunctions of amorphous and crystalline silicon. J. Non Cryst. Solids 299–302, 663–667. https://doi.org/10.1016/S0022-3093(01)01029-8.

[8] Garcia-Belmonte, G., García-Cañadas, J., Mora-Seró, I., Bisquert, J., Voz, C., Puigdollers, J., Alcubilla, R., 2006. Effect of buffer layer on minority carrier lifetime and series resistance of bifacial heterojunction silicon solar cells analyzed by impedance spectroscopy. Thin Solid Films 514, 254–257. https://doi.org/10.1016/j.tsf.2006.02.020.

[9] Garland, J.E., Crain, D.J., Roy, D., 2011. Impedance spectroscopy coupled with voltammetry for quantitative evaluation of temperature and voltage dependent parameters of a silicon solar cell. Sol. Energy 85, 2912–2923. https://doi.org/10.1016/j.solener.2011.08.029.

[10] Garland, J.E., Crain, D.J., Zheng, J.P., Sulyma, C.M., Roy, D., 2011. Electro-analytical characterization of photovoltaic cells by combining voltammetry and impedance spectroscopy: Voltage dependent parameters of a silicon solar cell under controlled illumination and temperature. Energ. Environ. Sci. 4, 485–498. https://doi.org/10.1039/c0ee00307g.

[11] Hirschorn, B., Orazem, M.E., Tribollet, B., Vivier, V., Frateur, I., Musiani, M., 2010. Determination of effective capacitance and film thickness from constant-phase-element parameters. Electrochim. Acta 55, 6218–6227. https://doi.org/10.1016/j.electacta.2009.10.065.

[12] Kleider, J.P., 2012. Band Lineup Theories and the Determination of Band Offsets from Electrical Measurements. Eng. Mater. 405–444 https://doi.org/10.1007/978-3-642-22275-7_12.

[13] Klein, A., Körber, C., Wachau, A., Säuberlich, F., Gassenbauer, Y., Harvey, S.P., Proffit, D.E., Mason, T.O., 2010. Transparent conducting oxides for photovoltaics: Manipulation of Fermi level, work function and energy band alignment. Materials (Basel). 3, 4892–4914. https://doi.org/10.3390/ma3114892.

[14] Kochowski, S., Nitsch, K., 2002. Description of the frequency behaviour of metal-SiO2-GaAs structure characteristics by electrical equivalent circuit with constant phase element. Thin Solid Films 415, 133–137. https://doi.org/10.1016/S0040-6090(02)00506-0.

[15] Kumar, S., Singh, P.K., Chilana, G.S., 2009. Study of silicon solar cell at different intensities of illumination and wavelengths using impedance spectroscopy. Sol. Energy Mater. Sol. Cells 93, 1881–1884. https://doi.org/10.1016/j.solmat.2009.07.002.

[16] Lasia, A., 2022. The Origin of the Constant Phase Element. J. Phys. Chem. Lett. 13, 580–589. https://doi.org/10.1021/acs.jpclett.1c03782.

[17] Miyano, K., Yanagida, M., Tripathi, N., Shirai, Y., 2015. Simple characterization of electronic processes in perovskite photovoltaic cells. Appl. Phys. Lett. 106 (9), 093903.

[18] Mora-Seró, I., Bisquert, J., Fabregat-Santiago, F., Garcia-Belmonte, G., Zoppi, G., Durose, K., Proskuryakov, Y., Oja, I., Belaidi, A., Dittrich, T., Tena-Zaera, R., Katty, A., Lévy-Clément, C., Barrioz, V., Irvine, S.J.C., 2006. Implications of the Negative Capacitance Observed at Forward Bias in Nanocomposite and Polycrystalline Solar Cells. Nano Lett. 6, 640–650. https://doi.org/10.1021/nl052295q.

[19] Mora-Seró, I., Garcia-Belmonte, G., Boix, P.P., Vázquez, M.A., Bisquert, J., 2009. Impedance spectroscopy characterisation of highly efficient silicon solar cells under different light illumination intensities. Energ. Environ. Sci. 2, 678. https://doi.org/10.1039/b812468j.

[20] Mora-Seró, I., Luo, Y., Garcia-Belmonte, G., Bisquert, J., Muñoz, D., Voz, C., Puigdollers, J., Alcubilla, R., 2008. Recombination rates in heterojunction silicon solar cells analyzed by impedance spectroscopy at forward bias and under illumination. Sol. Energy Mater. Sol. Cells 92, 505–509. https://doi.org/10.1016/j.solmat.2007.11.005.

[21] Mudgal, S., Singh, S., Komarala, V.K., 2020. Analysis of Process-Dependent Electrical Properties of Silicon Heterojunction Solar Cells by Quantum Efficiency and Temperature-Dependent Current Density-Voltage Measurements. Phys. Status Solidi A 217, 1900782. https://doi.org/10.1002/pssa.201900782.

[22] Pandey, A., Bhattacharya, S., Panigrahi, J., Mandal, S., Komarala, V.K., 2022. Effect of Gas Flow Rate in PECVD of Amorphous Silicon Thin Films for Interface Passivation of Silicon Heterojunction Solar Cells. Phys. Status Solidi A 219, 2200183. https://doi.org/10.1002/pssa.202200183.

[23] Panigrahi, J., Komarala, V.K., 2021. Progress on the intrinsic a-Si: H films for interface passivation of silicon heterojunction solar cells: A review. J. Non Cryst. Solids 574, 121166. https://doi.org/10.1016/j.jnoncrysol.2021.121166.

[24] Panigrahi, J., Vandana, Singh, R., Batra, N., Gope, J., Sharma, M., Pathi, P., Srivastava, S.K., Rauthan, C.M.S., Singh, P.K., 2016. Impedance spectroscopy of crystalline silicon solar cell: Observation of negative capacitance. Sol. Energy 136, 412–420.

[25] Perny, M., Saly, V., Vary, M., Mikolasek, M., Huran, J., 2015. Electrical characterization of a-SiC/c-Si solar cell structures, in: 2015 38th International Spring Seminar on Electronics Technology (ISSE). IEEE, pp. 16–20. doi: 10.1109/ISSE.2015.7247953.

[26] Powell, M.J., Deane, S.C., 1993. Improved defect-pool model for charged defects in amorphous silicon. Phys. Rev. B 48, 10815–10827. https://doi.org/10.1103/PhysRevB.48.10815.

[27] Pysch, D., Mette, A., Glunz, S.W., 2007. A review and comparison of different methods to determine the series resistance of solar cells. Sol. Energy Mater. Sol. Cells 91, 1698–1706. https://doi.org/10.1016/j.solmat.2007.05.026.

[28] Rißland, S., Breitenstein, O., 2013. Considering the distributed series resistance in a two-diode model. Energy Procedia 38, 167–175. https://doi.org/10.1016/j.egypro.2013.07.264.

[29] Ritzau, K.U., Bivour, M., Schröer, S., Steinkemper, H., Reinecke, P., Wagner, F., Hermle, M., 2014. TCO work function related transport losses at the a-Si:H/TCO-contact in SHJ solar cells. Sol. Energy Mater. Sol. Cells 131, 9–13. https://doi.org/10.1016/j.solmat.2014.06.026.

[30] Schulze, T.F., Korte, L., Conrad, E., Schmidt, M., Rech, B., 2010. Electrical transport mechanisms in a-Si:H/c-Si heterojunction solar cells. J. Appl. Phys. 107 (2), 023711.

[31] Suresh, M.S., 1996. Measurement of solar cell parameters using impedance spectroscopy. Sol. Energy Mater. Sol. Cells 43, 21–28. https://doi.org/10.1016/0927-0248(95)00153-0.

[32] Simon, S.M., Kwok, N.K., 2007. Physics of Semiconductor Devices, 3rd ed. Wiley, Hoboken, pp. 79–133.

[33] Taguchi, M., Kawamoto, K., Tsuge, S., Baba, T., Sakata, H., Morizane, M., Uchihashi, K., Nakamura, N., Kiyama, S., Oota, O., 2000. HITTM cells high-efficiency crystalline Si cells with novel structure. Prog. Photovolt. Res. Appl. 8, 503–513. https://doi.org/10.1002/1099-159X(200009/10)8:5<503::AID-PIP347>3.0.CO;2-G.

[34] Taguchi, M., Maruyama, E., Tanaka, M., 2008. Temperature dependence of amorphous/crystalline silicon heterojunction solar cells. Jpn. J. Appl. Phys. 47, 814–818. https://doi.org/10.1143/JJAP.47.814.

[35] Taguchi, M., Terakawa, A., Maruyama, E., Tanaka, M., 2005. Obtaining a higherVoc in HIT cells. Prog. Photovolt. Res. Appl. 13, 481–488. https://doi.org/10.1002/pip.646.

[36] van der Heide, A.S.H., Schönecker, A., Bultman, J.H., Sinke, W.C., 2005. Explanation of high solar cell diode factors by nonuniform contact resistance. Prog. Photovolt. Res. Appl. 13, 3–16. https://doi.org/10.1002/pip.556.

[37] Varache, R., Kleider, J.P., Gueunier-Farret, M.E., Korte, L., 2013. Silicon heterojunction solar cells: Optimization of emitter and contact properties from analytical calculation and numerical simulation. Mater. Sci. Eng. B Solid-State Mater. Adv. Technol. 178, 593–598. https://doi.org/10.1016/j.mseb.2012.11.011.

[38] von Hauff, E., 2019. Impedance Spectroscopy for Emerging Photovoltaics. J. Phys. Chem. C 123, 11329–11346. https://doi.org/10.1021/acs.jpcc.9b00892.

[39] Walter, T., Herberholz, R., Müller, C., Schock, H.W., 1996. Determination of defect distributions from admittance measurements and application to Cu(In, Ga)Se2 based heterojunctions. J. Appl. Phys. 80, 4411–4420. https://doi.org/10.1063/1.363401.

[40] Wang, J., 1990. Construction of CPA admittance with distributions of series rc-pairs. Solid State Ion. 39, 277–281. https://doi.org/10.1016/0167-2738(90)90407-I.